

2-9-2017

## Energetics of the S<sub>2</sub> State Spin Isomers of the Oxygen-Evolving Complex of Photosystem II

David J. Vinyard  
*Yale University*

Sahr Khan  
*Yale University*

Mikhail Askerka  
*Yale University*

Victor S. Batista  
*Yale University*

Gary W. Brudvig  
*Yale University*

Follow this and additional works at: [https://digitalcommons.lsu.edu/biosci\\_pubs](https://digitalcommons.lsu.edu/biosci_pubs)

---

### Recommended Citation

Vinyard, D., Khan, S., Askerka, M., Batista, V., & Brudvig, G. (2017). Energetics of the S<sub>2</sub> State Spin Isomers of the Oxygen-Evolving Complex of Photosystem II. *Journal of Physical Chemistry B*, 121 (5), 1020-1025. <https://doi.org/10.1021/acs.jpccb.7b00110>

This Article is brought to you for free and open access by the Department of Biological Sciences at LSU Digital Commons. It has been accepted for inclusion in Faculty Publications by an authorized administrator of LSU Digital Commons. For more information, please contact [ir@lsu.edu](mailto:ir@lsu.edu).

## Energetics of the S State Spin Isomers of the Oxygen-Evolving Complex of Photosystem II

David J. Vinyard, Sahr Khan, Mikhail Askerka, Victor S. Batista, and Gary W. Brudvig

*J. Phys. Chem. B*, **Just Accepted Manuscript** • Publication Date (Web): 12 Jan 2017

Downloaded from <http://pubs.acs.org> on January 12, 2017

### Just Accepted

“Just Accepted” manuscripts have been peer-reviewed and accepted for publication. They are posted online prior to technical editing, formatting for publication and author proofing. The American Chemical Society provides “Just Accepted” as a free service to the research community to expedite the dissemination of scientific material as soon as possible after acceptance. “Just Accepted” manuscripts appear in full in PDF format accompanied by an HTML abstract. “Just Accepted” manuscripts have been fully peer reviewed, but should not be considered the official version of record. They are accessible to all readers and citable by the Digital Object Identifier (DOI®). “Just Accepted” is an optional service offered to authors. Therefore, the “Just Accepted” Web site may not include all articles that will be published in the journal. After a manuscript is technically edited and formatted, it will be removed from the “Just Accepted” Web site and published as an ASAP article. Note that technical editing may introduce minor changes to the manuscript text and/or graphics which could affect content, and all legal disclaimers and ethical guidelines that apply to the journal pertain. ACS cannot be held responsible for errors or consequences arising from the use of information contained in these “Just Accepted” manuscripts.



# Energetics of the $S_2$ State Spin Isomers of the Oxygen-Evolving Complex of Photosystem II

David J. Vinyard,<sup>‡,§</sup> Sahr Khan,<sup>‡,†</sup> Mikhail Askerka, Victor S. Batista, and Gary W. Brudvig\*

Department of Chemistry, Yale University, New Haven, Connecticut, 06520-8107, United States

## ABSTRACT

The  $S_2$  redox intermediate of the oxygen-evolving complex in Photosystem II is present as two spin isomers. The  $S = 1/2$  isomer gives rise to a multiline EPR signal at  $g = 2$ , while the  $S = 5/2$  isomer exhibits a broad EPR signal at  $g = 4.1$ . The electronic structures of these isomers are known, but their role in the catalytic cycle of water oxidation remains unclear. We show that formation of the  $S = 1/2$  state from the  $S = 5/2$  state is exergonic at temperatures above 160 K. However, the  $S = 1/2$  isomer decays to  $S_1$  more slowly than the  $S = 5/2$  isomer. These differences support the hypotheses that the  $S_3$  state is formed via the  $S_2$  state  $S = 5/2$  isomer and that the stabilized  $S_2$  state  $S = 1/2$  isomer plays a role in minimizing  $S_2Q_A^-$  decay in light-limiting conditions.

## INTRODUCTION

In the catalytic cycle of the oxygen-evolving complex (OEC) of Photosystem II (PSII), redox intermediates of the  $\text{Mn}_4\text{CaO}_5$  complex are known as  $S_i$  states ( $i = 0-4$ ).<sup>1</sup> In each turn of the  $S$ -state cycle, four oxidizing equivalents generated by photochemical charge separation events are used to oxidize two water molecules forming one molecule of  $\text{O}_2$  and reducing two molecules of plastoquinone to plastoquinol. Protons taken from the stroma and released to the lumen contribute to the trans-membrane proton-motive force.<sup>2</sup>

The structure of the OEC in the dark-stable  $S_1$  state has been determined using a combination of X-ray crystallography,<sup>3,4</sup> extended X-ray absorption fine structure (EXAFS) spectroscopy,<sup>5,6</sup> and quantum mechanical (QM) calculations.<sup>7-10</sup> Multiple lines of evidence (reviewed in reference<sup>11</sup>) suggest that the  $S_1$  state contains two  $\text{Mn}^{3+}$  and two  $\text{Mn}^{4+}$ . However, an alternative hypothesis asserts that the  $S_1$  state contains either  $(\text{Mn}^{3+})_4$  or  $(\text{Mn}^{2+})(\text{Mn}^{3+})_2(\text{Mn}^{4+})$ .<sup>12, 13</sup>

The  $S_2$  state is produced from the  $S_1$  resting state by either continuous illumination at 130-220 K<sup>14, 15</sup> or by a single-turnover flash at ambient temperature.<sup>1, 16</sup> The  $S_2$  state is paramagnetic and has been extensively studied by using electron paramagnetic resonance (EPR) and EXAFS spectroscopies.<sup>17</sup> No proton is released during the  $S_1$  to  $S_2$  transition and one Mn ion is oxidized from  $\text{Mn}^{3+}$  to  $\text{Mn}^{4+}$ . The remaining  $\text{Mn}^{3+}$  center in the OEC in the  $S_2$  state can be present at the Mn1 or Mn4 positions (see Figure 1 for numbering). When Mn4 is  $\text{Mn}^{3+}$ , the OEC has a “closed cubane” motif and the ground spin state ( $S$ ) is 5/2 (Figure 1A). When Mn1 is  $\text{Mn}^{3+}$ , the OEC is in an “open cubane” form and the ground spin state is 1/2 (Figure 1B).<sup>9</sup> The  $S = 5/2$  spin isomer produces a nearly isotropic EPR signal at approximately  $g = 4.1$ ,<sup>14, 18</sup> while the  $S = 1/2$  spin isomer produces a “multiline” EPR spectrum centered at  $g = 2.0$  (Figure 1C).<sup>16</sup>

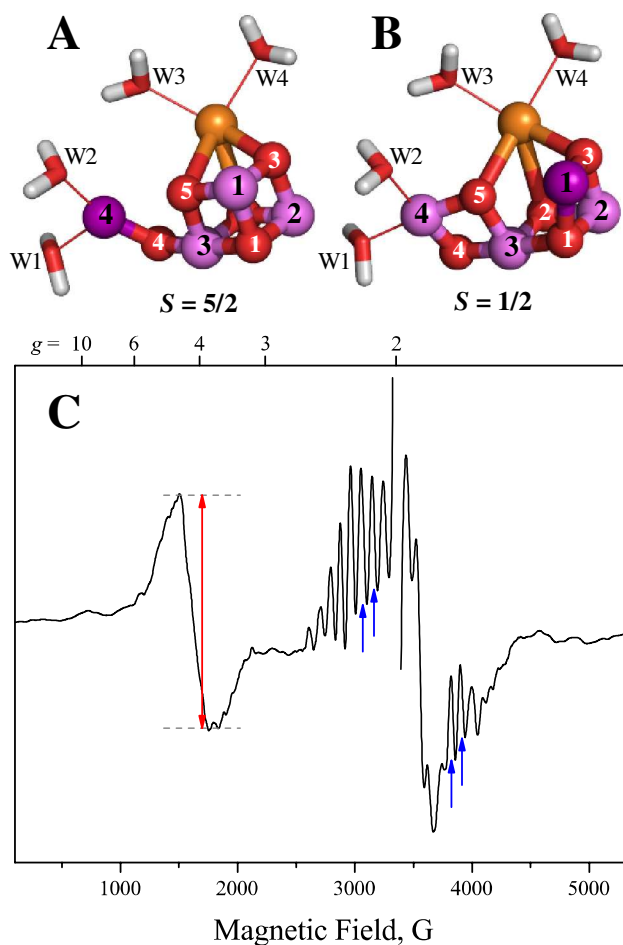


**Figure 1.** QM/MM optimized structures of the  $S_2$  state spin isomers with ground states of  $S = 5/2$  (A)<sup>19</sup> and  $S = 1/2$  (B)<sup>20</sup> (see Pantazis *et al.*<sup>9</sup>)  $Mn^{3+}$  ions are shown in purple,  $Mn^{4+}$  in lavender,  $Ca^{2+}$  in orange, and  $O^{2-}$  in red. (C) The  $S = 5/2$  isomer is characterized by a broad EPR signal at  $g = 4.1$  and the  $S = 1/2$  isomer gives rise to a multiline EPR signal centered at  $g = 2$ . The intensity of the  $g = 4.1$  signal is measured as the peak-to-peak height indicated by the red arrow. The intensity of the  $g = 2$  signal is determined by summing the peak-to-peak heights of the four features indicated by blue arrows.

Both spin isomers are present in PSII membranes isolated from higher plants. However, the relative intensities of the two EPR signals ( $g = 4.1$  and  $g = 2.0$ ) are sensitive to experimental

1  
2  
3 conditions such as the illumination temperature and choice of cryoprotectant.<sup>17</sup> In native  
4  
5 cyanobacterial PSII core complexes, only the  $S = 1/2$  spin isomer is observed.  
6  
7

8  
9 While the electronic structures of the two  $S_2$  spin isomers have been established by both  
10  
11 experiment<sup>21</sup> and theory,<sup>9</sup> the relative energetics have not been established. Herein, we  
12  
13 experimentally determine that the  $S = 1/2$  isomer is approximately  $0.7 \text{ kcal mol}^{-1}$  more stable than  
14  
15 the  $S = 5/2$  isomer, consistent with QM/MM calculations and discuss the chemical mechanism of  
16  
17 photosynthetic water oxidation in light of this finding.  
18  
19

## 20 21 22 **METHODS** 23

24  
25 Spinach PSII membranes were prepared as previously described<sup>22, 23</sup> and suspended to final  
26  
27 chlorophyll concentrations of  $5\text{-}8 \text{ mg mL}^{-1}$  in 50 mM MES, 20 mM  $\text{Ca}(\text{OH})_2$ , 10 mM NaCl,  
28  
29 0.01% Triton X-100, and 400 mM sucrose. The pH was adjusted to 6.0 with NaOH.  
30  
31

32  
33 EPR spectra were recorded using a Bruker ELEXSYS E500 spectrometer equipped with a SHQ  
34  
35 cavity and an Oxford ESR-900 helium flow cryostat at 6-7 K. Instrument parameters were  
36  
37 microwave frequency, 9.39 GHz; microwave power, 5 mW; modulation frequency, 100 kHz;  
38  
39 modulation amplitude, 19.5 G; sweep time, 84 s; conversion time, 41 ms; time constant, 82 ms.  
40  
41

42  
43 For  $S_2$  state conversion experiments, 0.5 mM phenyl-*p*-benzoquinone (PPBQ) was added to each  
44  
45 EPR sample from a 50 mM stock solution in dimethyl sulfoxide (DMSO). EPR samples were  
46  
47 illuminated in a quartz nitrogen flow cell at 135 K using a white xenon lamp supplemented with  
48  
49 a near-IR LED ( $\lambda_{\text{max}} = 850 \text{ nm}$ ). After four minutes, the sample was quickly removed to liquid  
50  
51 nitrogen (77 K) in darkness and transferred to the EPR cryostat. For incubations  $< 190 \text{ K}$ , the  
52  
53  
54  
55  
56  
57  
58  
59  
60

1  
2  
3 sample was returned to the nitrogen flow cell. For incubations  $\geq 195$  K, the sample was  
4 transferred to an equilibrated bath of varying ratios of ethanol/ethylene glycol in dry ice.  
5  
6

7  
8  
9 For  $S_2Q_A^-$  decay experiments, 0.5 mM 3-(3,4-dichlorophenyl)-1,1-dimethylurea (DCMU) was  
10 added to each EPR sample from a 50 mM stock solution in DMSO. EPR samples were  
11 illuminated in an ethanol/dry ice bath (200 K) using a white xenon lamp supplemented with a  
12 near-IR LED ( $\lambda_{\max} = 850$  nm). After four minutes, the sample was quickly removed to liquid  
13 nitrogen (77 K) in darkness and transferred to the EPR cryostat. For all incubations, the sample  
14 was transferred to an equilibrated bath of varying ratios of ethanol/ethylene glycol in dry ice.  
15  
16  
17  
18  
19  
20  
21  
22

23  
24 For both experiments, incubations were performed in complete darkness and the temperature was  
25 continuously monitored by using an external thermocouple.  
26  
27  
28

29  
30 EPR spectra subtractions and curve fittings were performed in OriginPro 9.1. Temperature  
31 fluctuations during EPR measurements were  $\pm 0.1$  K leading to subtraction errors specifically in  
32 the  $g \approx 4$  region due to rhombic iron contamination. These errors may affect EPR signal intensity  
33 measurements (Figure 1C) and are the predominant source of uncertainty in the values we report.  
34  
35  
36  
37  
38  
39  
40 Non-linear and linear curve fittings were performed in OriginPro using the Levenberg-Marquardt  
41 algorithm. Energy-minimized parameter values and associated standard errors are reported. For  
42 logarithmic plots, error bars span the natural logarithm of the mean  $\pm$  standard error.  
43  
44  
45  
46  
47

48 QM/MM calculations were performed as previously described<sup>8, 19, 20, 24</sup> using the B3LYP  
49 functional<sup>25, 26</sup> with the LANL2DZ pseudo-potential<sup>27, 28</sup> for Ca and Mn and the 6-31G\* basis  
50 set<sup>29</sup> for all other atoms for geometry optimizations and 6-311+G\*\* for energy evaluations. The  
51 choice of the high layer and the MM layer was done according to the scheme described in our  
52 previous models.<sup>20</sup> The AMBER force field was used for all MM layer atoms.<sup>30</sup>  
53  
54  
55  
56  
57  
58  
59  
60

## RESULTS AND DISCUSSION

To study the kinetics of conversion of the  $S = 5/2$  isomer to the  $S = 1/2$  isomer, we illuminated dark-adapted PSII membranes isolated from spinach containing the exogenous electron acceptor PPBQ and sucrose as a cryoprotectant at 135 K. Under those conditions, only the  $g = 4.1$  EPR signal is observed (Figure 2A)<sup>14</sup> because of the presence of near IR light during illumination<sup>31</sup> (see Methods). After an initial EPR spectrum was obtained, the same sample was incubated in total darkness at 150-242 K, which led to the conversion of the  $g = 4.1$  to the  $g = 2$  signal. For temperatures  $\leq 170$  K, the initial rate of conversion could be determined using this method (Figure 2B). The Arrhenius analysis of the rate constants predicts an activation barrier of  $6.7 \pm 0.5$  kcal mol<sup>-1</sup> (Figure 2C). This barrier is in close agreement with a previous study by de Paula *et al.* that reported an activation barrier of  $7.9 \pm 1.4$  kcal mol<sup>-1</sup> for this conversion under similar conditions.<sup>32</sup>

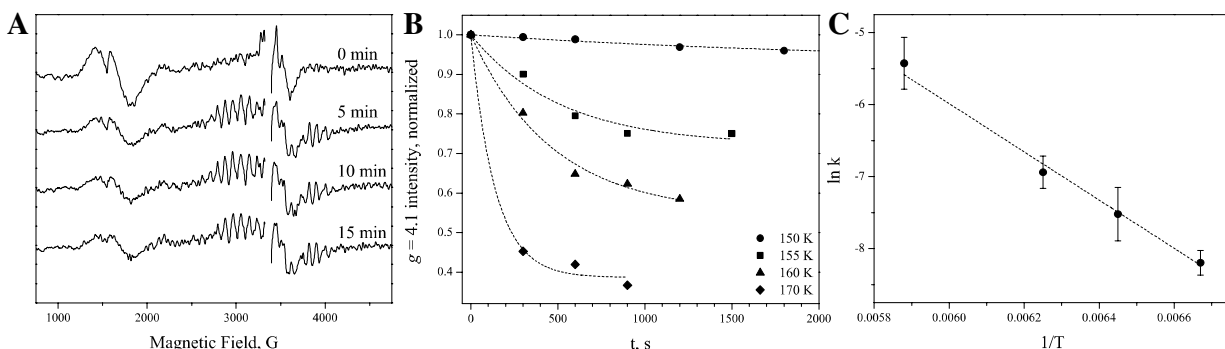


**Figure 2.** Kinetics of  $S_2$  state conversion. (A) Only the  $g = 4.1$  EPR signal is formed upon illumination at 135 K as shown in the light-*minus*-dark spectrum (top trace). During incubation in darkness at the representative temperature of 170 K in the presence of PPBQ, the  $g = 4.1$  EPR signal decreases in intensity and the  $g = 2$  EPR signal increases in intensity. Unsubtracted spectra are shown in Figure S1 of the Supporting Information. (B) Normalized peak-to-peak height of the  $g = 4.1$  EPR signal vs. incubation time. Data were fit to a single exponential decay function



( $y = y_0 + A \cdot \exp(-x/t)$ ) (dotted lines). (C) Arrhenius treatment of the data in panel B. Error bars represent standard error of the fit.  $E_a = 6.7 \pm 0.5 \text{ kcal mol}^{-1}$ ,  $A = 1.6 \pm 0.2 \times 10^6 \text{ s}^{-1}$ ,  $R^2 = 0.9867$ .

For all tested temperatures, the  $g = 4.1$  EPR signal decreased and the  $g = 2$  EPR signal increased during dark incubation. This behavior has been previously reported by multiple groups.<sup>14, 31-33</sup>

The  $g = 4.1$  signal intensity did not approach zero for extended incubation times (Figures 2A and 2B). Instead, the data suggest that a temperature-dependent equilibrium is established (see<sup>31, 34</sup>).

For temperatures  $> 170 \text{ K}$ , the  $g = 4.1$  signal decayed to a steady-state level in less than 300 s

(first time point in Figure 2B). While we could not determine the rates of  $S_2$  state conversion in

this temperature range due to fast conversion, equilibrium constants (defined here as

$K_{\text{eq}} = [g = 2.0]/[g = 4.1]$ ) could be measured. As shown in Figure 3,  $K_{\text{eq}}$  is biphasic with respect

to temperature. At temperatures  $< 170 \text{ K}$ , the van't Hoff treatment of the data provides a  $\Delta H^\circ$  of

$+31 \text{ kJ mol}^{-1}$  and a  $\Delta S^\circ$  of  $+190 \text{ J mol}^{-1} \text{ K}^{-1}$ . At temperatures  $\geq 195 \text{ K}$ , the conversion of the

$S = 5/2$  isomer to the  $S = 1/2$  isomer is thermodynamically less demanding ( $\Delta H^\circ = +0.40 \text{ kJ mol}^{-1}$

and  $\Delta S^\circ = +11 \text{ J mol}^{-1} \text{ K}^{-1}$ ) and becomes exergonic for temperatures  $> 160 \text{ K}$  (Figure S2). When

the data are extrapolated to 298 K, the equilibrium constant is estimated to be  $3.2 \pm 0.4$ ,

corresponding to  $\Delta G^\circ = -0.69 \pm 0.14 \text{ kcal mol}^{-1}$ .

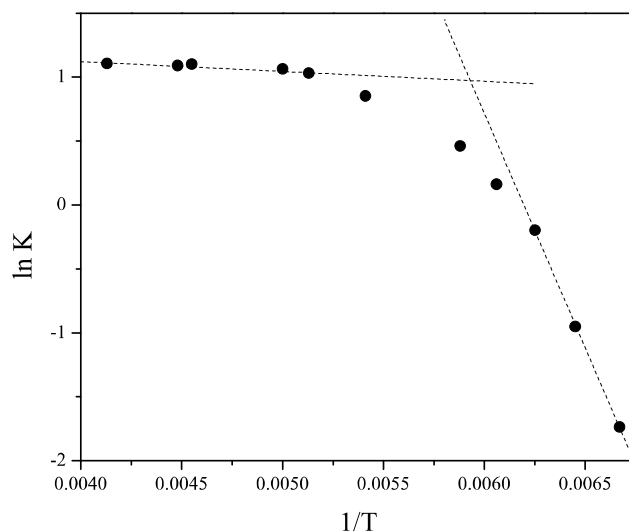


**Figure 3.** Temperature dependence of the equilibrium between  $S_2$  states. van't Hoff treatment of  $K_{eq}$  (defined as  $[g = 2.0]/[g = 4.1]$ ) shows two distinct linear regions. Fitted parameters are described in the text.

The biphasic temperature dependence of the  $S_2$  state spin isomer conversion may be caused by the surrounding protein environment. Extensive hydrogen-bonding networks involving water molecules, chloride, amino acid side chains and the protein backbone amides surround the OEC and influence its properties.<sup>35</sup> For example, a second shell water ligand labeled Wx is proposed to play a key role in water delivery to the OEC upon formation of the  $S_3$  state.<sup>19, 36</sup> As shown in Figure 4, Wx is a hydrogen-bond donor to the OEC in QM/MM structures of the  $S_1$  state and the  $S_2$  state  $S = 5/2$  isomer. However, this hydrogen bond is broken upon formation of the  $S_2$  state  $S = 1/2$  isomer due to a dramatic decrease of the  $\mu$ -oxo (O4)  $pK_a$  upon oxidation of Mn4 from  $Mn^{3+}$  to  $Mn^{4+}$ . We propose that the curvature in the data in Figure 3 reveals a ‘glass transition’ of the local environment around the OEC. At low temperatures, hydrogen-bonding interactions are frozen in place and only the  $S = 5/2$  isomer can be formed from the  $S_1$  state. However, at elevated temperatures above the glass transition, the hydrogen-bonding network can rearrange to

accommodate the thermodynamically preferred  $S = 1/2$  isomer. An H/D kinetic isotope effect of 2.5 associated with the conversion of the  $S_2$  spin states at 160 K (Figure S3) further supports this hypothesis. Previous studies by Boussac and coworkers have shown that the  $g = 4.1$  EPR signal formed by near IR illumination at 77-160 K is different from the  $g = 4.1$  EPR signal formed by 200 K illumination in terms of its temperature stability.<sup>31, 33, 34, 37</sup> We propose that the changes in hydrogen-bonding networks above the observed glass transition may be responsible for this behavior.

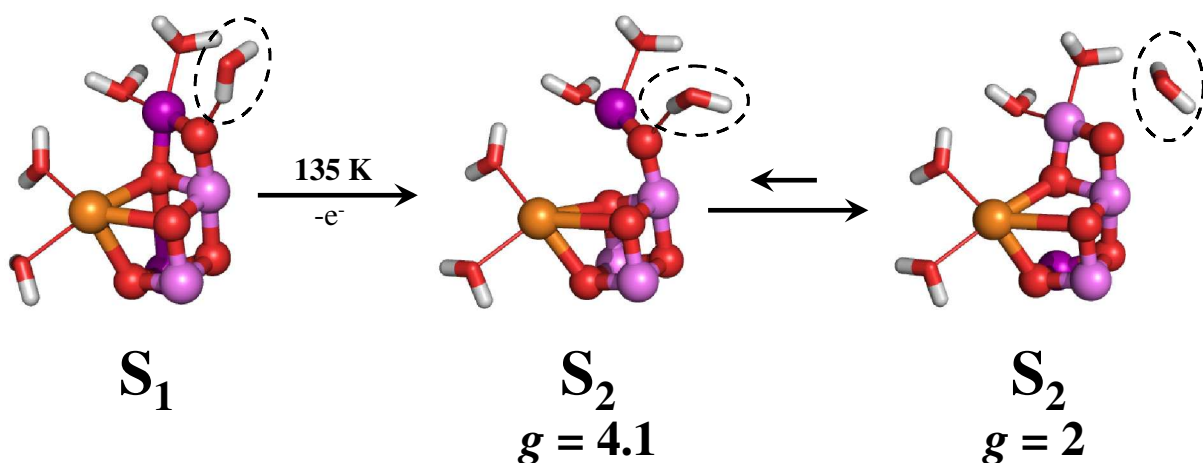


**Figure 4.** QM/MM optimized structures of the  $S_1$  state and the two spin isomers of the  $S_2$  state. Only the  $g = 4.1$  EPR signal corresponding to the  $S = 5/2$  spin isomer is formed at 135 K, but it spontaneously converts to the  $S = 1/2$  spin isomer at temperatures  $> 160$  K. The second shell water molecule,  $W_x$ , is circled in each structure.  $W_x$  is a hydrogen-bond donor to the OEC in the  $S_1$  state and the  $S = 5/2$  spin isomer of the  $S_2$  state, but not in the  $S = 1/2$  spin isomer of the  $S_2$  state.  $Mn^{3+}$  ions are shown in purple,  $Mn^{4+}$  in lavender,  $Ca^{2+}$  in orange, and  $O^{2-}$  in red.

To study the kinetics of the  $S_2Q_A^-$  state decaying to  $S_1Q_A$  by charge recombination, dark-adapted PSII samples containing the secondary acceptor,  $Q_B$  site inhibitor DCMU were illuminated at

200 K. Under these conditions, both the  $g = 4.1$  and  $g = 2.0$  EPR signals were observed (Figure 5A).<sup>15</sup> After an initial EPR spectrum was obtained, the same sample was incubated in total darkness at 218-258 K and the rates at which the  $g = 4.1$  and  $g = 2.0$  EPR signals decay were determined (Figure S4 in the Supporting Information). The  $g = 4.1$  EPR signal was found to decay faster than the  $g = 2.0$  signal. Arrhenius analysis of the rate constants provides an activation barrier for charge recombination of  $6.3 \pm 0.3$  kcal mol<sup>-1</sup> for the S<sub>2</sub> state  $g = 4.1$  spin isomer and  $10.5 \pm 0.9$  kcal mol<sup>-1</sup> for the S<sub>2</sub> state  $g = 2.0$  spin isomer (Figure 5B).

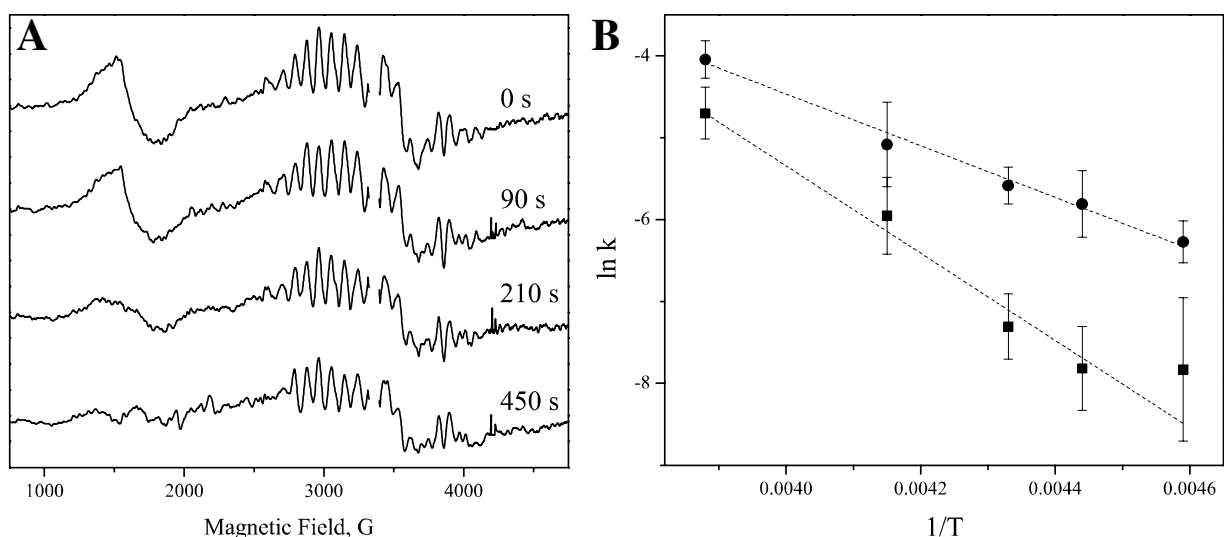


**Figure 5.** Kinetics of S<sub>2</sub>Q<sub>A</sub><sup>-</sup> decay to S<sub>1</sub>Q<sub>A</sub>. (A) Both the  $g = 4.1$  and the  $g = 2$  EPR signals are formed upon illumination at 200 K as shown in the light-*minus*-dark spectrum (top trace). During incubation in darkness at the representative temperature of 218 K in the presence of DCMU, the  $g = 4.1$  EPR signal decreases faster than the  $g = 2$  EPR signal. Unsubtracted spectra are shown in Figure S5 of the Supporting Information. (B) Arrhenius analysis of the decay kinetics of S<sub>2</sub>Q<sub>A</sub><sup>-</sup> to S<sub>1</sub>Q<sub>A</sub>. For the  $g = 4.1$  EPR signal (circles),  $E_a = 6.3 \pm 0.3$  kcal mol<sup>-1</sup>,  $A = 3.6 \pm 0.3 \times 10^3$  s<sup>-1</sup>,

1  
2  
3  $R^2 = 0.9924$ . For the  $g = 2$  EPR signal (squares),  $E_a = 10.5 \pm 0.9 \text{ kcal mol}^{-1}$ ,

4  
5  
6  $A = 8.8 \pm 1.1 \times 10^6 \text{ s}^{-1}$ ,  $R^2 = 0.9699$ .

7  
8  
9 These experiments revealed two key energetic features of the  $S_2$  state spin isomers: (1)  
10 conversion of the  $S = 5/2$  isomer to the  $S = 1/2$  isomer is exergonic at temperatures  $> 160 \text{ K}$ , and  
11  
12 (2) the  $S = 1/2$  isomer has an activation barrier approximately 67% higher for charge  
13  
14 recombination from  $S_2Q_A^-$  to form  $S_1Q_A$  than the  $S = 5/2$  isomer.  
15  
16  
17

18  
19  
20 Several computational chemistry groups have estimated the relative energetics of the  $S_2$  state  
21  
22 spin isomers. Pantazis, Neese and coworkers first used QM calculations to determine that the  
23  
24  $S = 1/2$  isomer was more stable than the  $S = 5/2$  isomer by  $0.42 - 1.64 \text{ kcal mol}^{-1}$ .<sup>9</sup> Similar results  
25  
26 have been shown by Yamaguchi and coworkers ( $1.3 \text{ kcal mol}^{-1}$ )<sup>38</sup> and Kaila and coworkers  
27  
28 ( $1.1 \text{ kcal mol}^{-1}$ ).<sup>39</sup> Guidoni *et al.* have used QM/MM-MD methods to determine that the  $\Delta G$  at  
29  
30 298 K between the  $S_2$  state isomers is  $1.1 \text{ kcal mol}^{-1}$  with the  $S = 1/2$  isomer being more stable.<sup>40</sup>  
31  
32 Using QM/MM methods and models described in the Supporting Information, we find that the  
33  
34 energy of the  $S = 1/2$  isomer is  $0.84 \text{ kcal mol}^{-1}$  lower than that of the  $S = 5/2$  isomer. All of these  
35  
36 theoretical findings are in excellent agreement with the experimental results in this work  
37  
38  
39  
40  
41 ( $\Delta G = -0.69 \pm 0.14 \text{ kcal mol}^{-1}$  at 298 K).  
42  
43

44  
45 The kinetics of formation of the  $S_2$  state and its conversion from  $S = 1/2$  spin isomer to the  
46  
47  $S = 5/2$  spin isomer and vice versa have been harder to determine computationally as the  
48  
49 transition involves both a change in the spin state and geometry. The reaction barriers we  
50  
51 measure provide this vital information needed to delineate the PSII water-oxidation reaction  
52  
53 coordinate.  
54  
55  
56  
57  
58  
59  
60

1  
2  
3 These data suggest that at ambient temperature (298 K) in higher plant PSII, approximately 75%  
4 of the  $S_2$  state population is in the  $S = 1/2$  spin isomer, while approximately 25% is in the  $S = 5/2$   
5 spin isomer. The excess  $S_2$  state population in the  $S = 1/2$  isomer decays more slowly to  $S_1$  via  
6 charge recombination with  $Q_A^-$ .  
7  
8  
9

10  
11  
12  
13 Previously, we and others have suggested that the  $S_3$  state is formed via the  $S_2$  state  $S = 5/2$   
14 isomer.<sup>19, 41</sup> This seems to be in contradiction to the fact that the equilibrium between the  $S_2$  spin  
15 isomers clearly favors the  $S = 1/2$  isomer at 298 K. However, depending on environmental light  
16 conditions, cyanobacteria, algae, and plants must carefully balance the thermodynamics of OEC  
17 advancement and charge recombination.<sup>42</sup> The distribution of  $S_2$  state spin isomers may thus play  
18 a role in regulating photosynthetic efficiency under light-limited conditions.<sup>43</sup> A majority of the  
19  $S_2$  state population remains in the stabilized low-spin isomer that has slower  $S_2Q_A^-$  charge  
20 recombination. A minority of the  $S_2$  state population is in the reactive high-spin isomer that has  
21 faster  $S_2Q_A^-$  charge recombination, but can advance to the  $S_3$  state. Balancing these two  
22 populations can thus tune the overall efficiency of PSII. Pantazis and coworkers and Guidoni and  
23 coworkers have used computational methods to show that the relative  $S_2$  spin isomer populations  
24 change when  $Y_Z$  is oxidized.<sup>41, 44</sup> While the influence of  $Y_Z$  is outside the scope of this study, it is  
25 likely an important factor in the  $S_2$  to  $S_3$  transition.  
26  
27  
28  
29  
30  
31  
32  
33  
34  
35  
36  
37  
38  
39  
40  
41  
42  
43  
44

## 45 CONCLUSIONS

46  
47  
48 We have determined the energetics of the  $S_2$  state spin isomers (summarized in Figure 6). The  $S_2$   
49 state spin isomer conversion experiments reveal that the free energy difference between the two  
50 ground spin states is  $0.69 \pm 0.14$  kcal mol<sup>-1</sup> at 298 K with the  $S = 1/2$  spin isomer being more  
51 stable.  $S_2Q_A^-$  decay experiments reveal that the  $S = 5/2$  spin isomer has a lower activation barrier  
52  
53  
54  
55  
56  
57  
58  
59  
60

for charge recombination to form  $S_1Q_A$  than the  $S = 1/2$  spin isomer. These differences support the hypotheses that the  $S_3$  state is formed from the  $S_2$  state  $S = 5/2$  spin isomer and that the stabilized  $S_2$  state  $S = 1/2$  spin isomer plays a role in minimizing  $S_2Q_A^-$  decay in light-limiting conditions. These findings provide experimental insights into the mechanism of natural water oxidation.

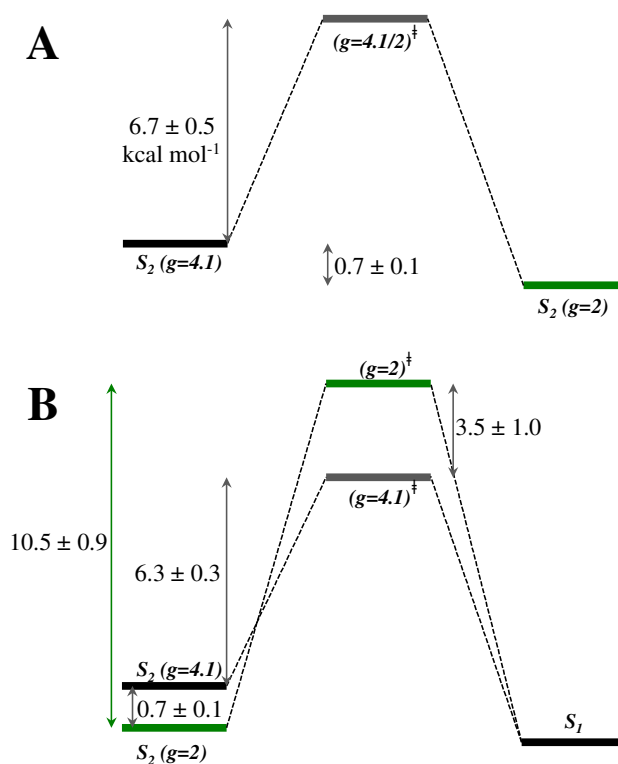


**Figure 6.** Compiled energetics schemes for (A) the conversion of the  $S_2$  state  $S = 5/2$  isomer to the  $S_2$  state  $S = 1/2$  isomer and (B) decay of the  $S_2Q_A^-$  state to  $S_1Q_A$  for both  $S_2$  state spin isomers.

## ASSOCIATED CONTENT

**Supporting Information.** The Supporting Information is available free of charge on the ACS Publications website (<http://pubs.acs.org>). This information includes figures showing

1  
2  
3 unsubtracted EPR spectra for Figures 2A and 5A, temperature-dependence of the free energy of  
4  
5  $S_2$  state spin isomer conversion,  $S_2$  state spin isomer conversion in  $D_2O$ , and  $S_2Q_A^-$  decay data at  
6  
7  
8 218 – 258 K.  
9

## 11 **AUTHOR INFORMATION**

### 14 **Corresponding Author**

16  
17 \*Email: gary.brudvig@yale.edu. Phone: (203) 432-5202. Fax: (203) 432-6144  
18  
19

### 20 **Present Addresses**

21  
22 § Department of Biological Sciences, Louisiana State University, Baton Rouge, Louisiana  
23  
24 70803, United States  
25  
26

27  
28 †Department of Chemistry, Massachusetts Institute of Technology, Cambridge, Massachusetts  
29  
30 02139, United States  
31  
32

### 33 **Author Contributions**

34  
35  
36  
37 ‡These authors contributed equally.  
38  
39

## 40 **ACKNOWLEDGMENT**

41  
42 The authors acknowledge support by the U.S. Department of Energy, Office of Science, Office  
43  
44 of Basic Energy Sciences, Division of Chemical Sciences, Geosciences, and Biosciences,  
45  
46 Photosynthetic Systems. Experimental work was funded by Grant DE-FG02-05ER15646  
47  
48 (G.W.B.) and computation work was funded by Grant DESC0001423 (V.S.B). We thank the  
49  
50 National Energy Research Scientific Computing Center (NERSC) and Shanghai Jiao Tong  
51  
52 University II High Performance Computation Center for generous computer time allocations. We  
53  
54  
55 thank Prof. Marilyn Gunner for helpful discussions.  
56  
57  
58  
59  
60



## REFERENCES

1. Kok, B.; Forbush, B.; McGloin, M., Cooperation of charges in photosynthetic O<sub>2</sub> evolution I. A linear four step mechanism. *Photochem. Photobiol.* **1970**, *11*, 457-475.
2. Blankenship, R. E., *Molecular Mechanisms of Photosynthesis*. 2nd ed.; John Wiley & Sons, Ltd.: Chichester, 2014.
3. Umena, Y.; Kawakami, K.; Shen, J.-R.; Kamiya, N., Crystal structure of oxygen-evolving photosystem II at a resolution of 1.9 Å. *Nature* **2011**, *473*, 55-60.
4. Suga, M.; Akita, F.; Hirata, K.; Ueno, G.; Murakami, H.; Nakajima, Y.; Shimizu, T.; Yamashita, K.; Yamamoto, M.; Ago, H., et al., Native structure of photosystem II at 1.95 Å resolution viewed by femtosecond X-ray pulses. *Nature* **2014**, *517*, 99-103.
5. Grundmeier, A.; Dau, H., Structural models of the manganese complex of photosystem II and mechanistic implications. *Biochim. Biophys. Acta - Bioenerg.* **2012**, *1817*, 88-105.
6. Sauer, K.; Yano, J.; Yachandra, V. K., X-ray spectroscopy of the photosynthetic oxygen-evolving complex. *Coord. Chem. Rev.* **2008**, *252*, 318-335.
7. Lubber, S.; Rivalta, I.; Umena, Y.; Kawakami, K.; Shen, J.-R.; Kamiya, N.; Brudvig, G. W.; Batista, V. S., S<sub>1</sub>-state model of the O<sub>2</sub>-evolving complex of photosystem II. *Biochemistry* **2011**, *50*, 6308-6311.
8. Pal, R.; Negre, C. F. A.; Vogt, L.; Pokhrel, R.; Ertem, M. Z.; Brudvig, G. W.; Batista, V. S., S<sub>0</sub>-state model of the oxygen-evolving complex of photosystem II. *Biochemistry* **2013**, *52*, 7703-7706.
9. Pantazis, D. A.; Ames, W.; Cox, N.; Lubitz, W.; Neese, F., Two interconvertible structures that explain the spectroscopic properties of the oxygen-evolving complex of photosystem II in the S<sub>2</sub> state. *Angew. Chem. Int. Ed.* **2012**, *51*, 9935-9940.
10. Siegbahn, P. E. M., Water oxidation mechanism in photosystem II, including oxidations, proton release pathways, O—O bond formation and O<sub>2</sub> release. *Biochim. Biophys. Acta - Bioenerg.* **2013**, *1827*, 1003-1019.
11. Vinyard, D. J.; Khan, S.; Brudvig, G. W., Photosynthetic water oxidation: Binding and activation of substrate waters for O-O bond formation. *Faraday Discuss.* **2015**, *185*, 37-50.
12. Vinyard, D. J.; Ananyev, G. M.; Dismukes, G. C., Photosystem II: The reaction center of oxygenic photosynthesis. *Ann. Rev. Biochem.* **2013**, *82*, 577-606.
13. Gatt, P.; Petrie, S.; Stranger, R.; Pace, R. J., Rationalizing the 1.9 Å crystal structure of photosystem II—A remarkable Jahn–Teller balancing act induced by a single proton transfer. *Angew. Chem. Int. Ed.* **2012**, *51*, 12025-12028.
14. Casey, J. L.; Sauer, K., EPR detection of a cryogenically photogenerated intermediate in photosynthetic oxygen evolution. *Biochim. Biophys. Acta - Bioenerg.* **1984**, *767*, 21-28.
15. de Paula, J. C.; Innes, J. B.; Brudvig, G. W., Electron transfer in photosystem II at cryogenic temperatures. *Biochemistry* **1985**, *24*, 8114-8120.
16. Dismukes, G. C.; Siderer, Y., Intermediates of a polynuclear manganese center involved in photosynthetic oxidation of water. *Proc. Natl. Acad. Sci., USA* **1981**, *78*, 274-278.
17. Pokhrel, R.; Brudvig, G. W., Oxygen-evolving complex of photosystem II: Correlating structure with spectroscopy. *Phys. Chem. Chem. Phys.* **2014**, *16*, 11812-11821.
18. Zimmermann, J. L.; Rutherford, A. W., Electron paramagnetic resonance properties of the S<sub>2</sub> state of the oxygen-evolving complex of photosystem II. *Biochemistry* **1986**, *25*, 4609-4615.

19. Askerka, M.; Vinyard, D. J.; Brudvig, G. W.; Batista, V. S., NH<sub>3</sub> binding to the S<sub>2</sub> state of the O<sub>2</sub>-evolving complex of photosystem II: Analogue to H<sub>2</sub>O binding during the S<sub>2</sub> → S<sub>3</sub> transition. *Biochemistry* **2015**, *54*, 5783-5786.
20. Askerka, M.; Wang, J.; Brudvig, G. W.; Batista, V. S., Structural changes in the oxygen-evolving complex of photosystem II induced by the S<sub>1</sub> to S<sub>2</sub> transition: A combined XRD and QM/MM study. *Biochemistry* **2014**, *53*, 6860-6862.
21. Chatterjee, R.; Han, G.; Kern, J.; Gul, S.; Fuller, F. D.; Garachtchenko, A.; Young, I. D.; Weng, T.-C.; Nordlund, D.; Alonso-Mori, R., et al., Structural changes correlated with magnetic spin state isomorphism in the S<sub>2</sub> state of the Mn<sub>4</sub>CaO<sub>5</sub> cluster in the oxygen-evolving complex of photosystem II. *Chem. Sci.* **2016**, *7*, 5236-5248.
22. Berthold, D. A.; Babcock, G. T.; Yocum, C. F., A highly resolved, oxygen-evolving photosystem II preparation from spinach thylakoid membranes. *FEBS letters* **1981**, *134*, 231-234.
23. Beck, W. F.; de Paula, J. C.; Brudvig, G. W., Active and resting states of the oxygen-evolving complex of photosystem II. *Biochemistry* **1985**, *24*, 3035-3043.
24. Askerka, M.; Vinyard, D. J.; Wang, J.; Brudvig, G. W.; Batista, V. S., Analysis of the radiation-damage-free X-ray structure of photosystem II in light of EXAFS and QM/MM data. *Biochemistry* **2015**, *54*, 1713-1716.
25. Becke, A. D., Density-functional exchange-energy approximation with correct asymptotic behavior. *Phys. Rev. A* **1988**, *38*, 3098-3100.
26. Becke, A. D., Density-functional thermochemistry. III. The role of exact exchange. *J. Chem. Phys.* **1993**, *98*, 5648-5652.
27. Hay, P. J.; Wadt, W. R., Ab initio effective core potentials for molecular calculations. Potentials for K to Au including the outermost core orbitals. *J. Chem. Phys.* **1985**, *82*, 299-310.
28. Wadt, W. R.; Hay, P. J., Ab initio effective core potentials for molecular calculations. Potentials for main group elements Na to Bi. *J. Chem. Phys.* **1985**, *82*, 284-298.
29. Hariharan, P. C.; Pople, J. A., The influence of polarization functions on molecular orbital hydrogenation energies. *Theoret. Chim. Acta* **1973**, *28*, 213-222.
30. Case, D. A.; Darden, T. A.; Cheatham, T. E.; Simmerling, C. L.; Wang, J.; Duke, R. E.; Luo, R.; Walker, R. C.; Zhang, W.; Merz, K. M., et al., AMBER 12. **2012**, University of California, San Francisco.
31. Boussac, A.; Girerd, J.-J.; Rutherford, A. W., Conversion of the spin state of the manganese complex in photosystem II induced by near-infrared light. *Biochemistry* **1996**, *35*, 6984-6989.
32. de Paula, J. C.; Beck, W. F.; Miller, A.-F.; Wilson, R. B.; Brudvig, G. W., Studies of the manganese site of photosystem II by electron spin resonance spectroscopy. *J. Chem. Soc., Faraday Trans. 1* **1987**, *83*, 3635-3651.
33. Boussac, A.; Un, S.; Horner, O.; Rutherford, A. W., High-spin states (S ≥ 5/2) of the photosystem II manganese complex. *Biochemistry* **1998**, *37*, 4001-4007.
34. Boussac, A.; Rutherford, A. W., Comparative study of the g=4.1 EPR signals in the S<sub>2</sub> state of photosystem II. *Biochim. Biophys. Acta - Bioenerg.* **2000**, *1457*, 145-156.
35. Vogt, L.; Vinyard, D. J.; Khan, S.; Brudvig, G. W., Oxygen-evolving complex of photosystem II: An analysis of second-shell residues and hydrogen-bonding networks. *Curr. Opin. Chem. Biol.* **2015**, *25*, 152-158.
36. Capone, M.; Narzi, D.; Bovi, D.; Guidoni, L., Mechanism of water delivery to the active site of photosystem II along the S<sub>2</sub> to S<sub>3</sub> transition. *J. Phys. Chem. Lett.* **2016**, *7*, 592-596.

- 1  
2  
3 37. Boussac, A.; Sugiura, M.; Kirilovsky, D.; Rutherford, A. W., Near-infrared-induced  
4 transitions in the manganese cluster of photosystem II: Action spectra for the S<sub>2</sub> and S<sub>3</sub> redox  
5 states. *Plant Cell Phys.* **2005**, *46*, 837-842.
- 6  
7 38. Isobe, H.; Shoji, M.; Shen, J.-R.; Yamaguchi, K., Strong coupling between the hydrogen  
8 bonding environment and redox chemistry during the S<sub>2</sub> to S<sub>3</sub> transition in the oxygen-evolving  
9 complex of Photosystem II. *J. Phys. Chem. B* **2015**, *119*, 13922-13933.
- 10  
11 39. Ugur, I.; Rutherford, A. W.; Kaila, V. R. I., Redox-coupled substrate water  
12 reorganization in the active site of photosystem II—The role of calcium in substrate water  
13 delivery. *Biochim. Biophys. Acta - Bioenerg.* **2016**, *1857*, 740-748.
- 14  
15 40. Bovi, D.; Narzi, D.; Guidoni, L., The S<sub>2</sub> state of the oxygen-evolving complex of  
16 photosystem II explored by QM/MM dynamics: Spin surfaces and metastable states suggest a  
17 reaction path towards the S<sub>3</sub> state. *Angew. Chem. Int. Ed.* **2013**, *52*, 11744-11749.
- 18  
19 41. Retegan, M.; Krewald, V.; Mamedov, F.; Neese, F.; Lubitz, W.; Cox, N.; Pantazis, D. A.,  
20 A five-coordinate Mn(IV) intermediate in biological water oxidation: spectroscopic signature  
21 and a pivot mechanism for water binding. *Chem. Sci.* **2016**, *7*, 72-84.
- 22  
23 42. Rutherford, A. W.; Osyczka, A.; Rappaport, F., Back-reactions, short-circuits, leaks and  
24 other energy wasteful reactions in biological electron transfer: Redox tuning to survive life in O<sub>2</sub>.  
25 *FEBS Letters* **2012**, *586*, 603-616.
- 26  
27 43. Krewald, V.; Retegan, M.; Neese, F.; Lubitz, W.; Pantazis, D. A.; Cox, N., Spin state as a  
28 marker for the structural evolution of nature's water-splitting catalyst. *Inorg. Chem.* **2016**, *55*,  
29 488-501.
- 30  
31 44. Narzi, D.; Bovi, D.; Guidoni, L., Pathway for Mn-cluster oxidation by tyrosine-Z in the  
32 S<sub>2</sub> state of photosystem II. *Proc. Natl. Acad. Sci., USA* **2014**, *111*, 8723-8728.
- 33  
34  
35  
36  
37  
38  
39  
40  
41  
42  
43  
44  
45  
46  
47  
48  
49  
50  
51  
52  
53  
54  
55  
56  
57  
58  
59  
60

## TOC GRAPHIC

